Residues surrounding the active centre of carbon monoxide dehydrogenase are key in converting CO_2 to CO

Umberto Terranova

Faculty of Medicine and Health Sciences, Crewe campus, University of Buckingham, Crewe, CW1 5DU, UK

Abstract

The enzyme carbon monoxide dehydrogenase is capable of efficiently converting CO_2 to CO and therefore can enable an affordable CO_2 recycling strategy. The reduction of CO_2 occurs at a peculiar nickel-iron-sulfur cluster, following a mechanism that remains little understood. In this study, we have used *ab initio* molecular dynamics simulations to explore the free energy landscape of the reaction. We predict the existence of a COOH ligand that strongly interacts with the surrounding protein residues and favours a mechanism where a H_2O molecule is eliminated before CO. We have taken advantages of the insights offered by our simulations to revisit the catalytic mechanism and the role of the residues surrounding the active centre in particular, thus assisting in the design of inorganic catalysts that mimic the enzyme.

1 Introduction

Global warming driven by the ever-increasing CO_2 emissions is one of the biggest challenges that we face. A promising solution to reduce the CO_2 concentration

in the atmosphere is the catalytic conversion of CO_2 into useful chemicals such as CO, methanol and ethanol[1,2]. However, due to the high stability of the CO_2 molecule, the utilisation of CO_2 is commonly possible only with expensive metal-based catalysts and therefore alternative approaches are required[3].

In nature, the enzyme carbon monoxide dehydrogenase (CODH) catalyses the reversible conversion of CO_2 to CO under physiological conditions[4]. Electrochemical studies have shown that the reaction occurs at a turnover rate of 0.2 s^{-1} and does not require any overpotential[5,6]. X-ray diffraction data have revealed that CODH is a homodimer whose subunits are bridged by a [4Fe–4S] cluster (D-cluster)[7–12]. Each subunit contains a [4Fe–4S] cluster (B-cluster) and a [Ni–4Fe–4S] cluster (C-cluster). It is in the C-cluster that the reduction of CO_2 occurs[13,14]. The C-cluster consists of a $NiFe_3S_4$ centre reminiscent of the Fe_4S_4 cubane cluster of the Fe protein[15] that is bridged to a unique external Fe atom[9,16], as shown in the upper panel of Figure 1.

Systems where CODH is coupled to a light-harvesting material represent a viable route to tackle global warming by artificial photosynthesis[17–19]. However, the extreme oxygen sensitivity of the enzyme[4] makes the design of inorganic catalysts with the unique features of the C-cluster and its surrounding residues extremely attractive[20,21]. In this context, the knowledge of the CODH reaction mechanism is crucial. For example, determining the rate-limiting step can enable fine-tuning the catalyst structure to accelerate the reaction. However, despite the significant contributions[11,22–26], the catalytic pathway leading to the formation of CO is not established yet.

Here, we use molecular dynamics simulations based on density functional theory (DFT) to explore the free energy landscape of the reaction. We show that a COOH, not a CO_2, ligand binds the reduced state of the C-cluster. Depending on which O atom initially participates in the reaction, we identify two possible mechanisms leading to the formation of CO and link them to the two different coordinations of Ni reported in the literature[9,11,16]. In both mechanisms, a H_2O molecule is released before CO. However, one mechanism is kinetically

more favourable than the other and thus we include it in a revised catalytic cycle that rationalises the role of the major residues surrounding the C-cluster.

2 Methods

2.1 Modelling the enzyme-substrate complex

We derived our model of CODH with CO_2 bound from the reduced structure of *Carboxydothermus hydrogenoformans* (PDB code 3B52)[11]. By cutting along the C–N peptide bonds, all the residues with at least one atom within 5.5 Å from the Ni atom were included in the model, which resulted formed by the C-cluster, CO_2, His93, His261, Lys563, Cys295, Cys333, Cys476, Cys526, Cys446, Gly475, Ile567, Wat1102 and Wat1887. The N-terminal sides were then capped with H atoms (NH_3^+) and the C-terminal sides with O atoms (COO^-). All missing hydrogen atoms were added with VMD[27]. Both N atoms of His93 were protonated (positively charged imidazole ring), while only the N atom of His261 not bound to the C-cluster was protonated (neutral imidazole ring). The final model contains 188 atoms and is illustrated in the lower panel of Figure 1.

2.2 Computational details

All DFT simulations were performed with the QUICKSTEP program of CP2K[28]. We used the PBE exchange-correlation functional[29], the DZVP-MOLOPT basis set[30], and the GTH pseudopotentials proposed by Goedecker, Teter and Hutter[31]. The antiferromagnetic coupling of the Fe atoms was treated by the broken symmetry approach[32]. In particular, Fe(II) and Fe2(II) ($S = 4$) were coupled with Fe3(II) and Fe4(III) ($S = 5/2$) to model the $S = 1/2$ electron paramagnetic resonance signal[33] (upper panel of Figure 1), as Amara *et al.* found that this combination best reproduces Mössbauer data[25]. With a zero oxidation state of Ni[11], assigning formal charges of +1 to the C-cluster , –2 to CO_2, +1 to His93, +1 to Lys563 and –1 to each of the five cysteines, results into a net charge of the model of –2.

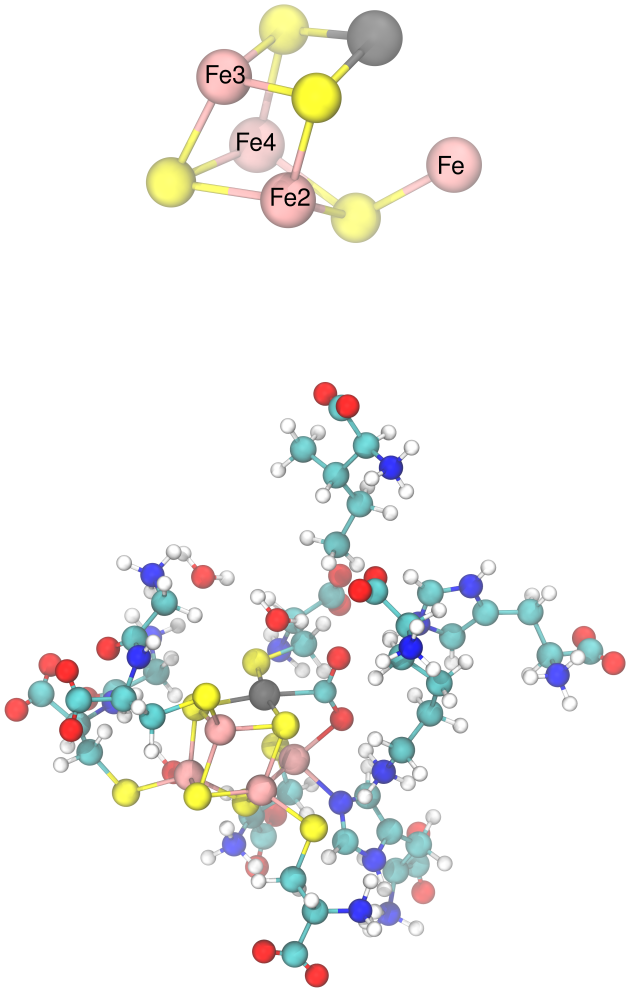

Figure 1: Upper panel: The C-cluster of CODH. The external iron atom has been labelled as Fe. Lower panel: The model of CODH with CO_2 bound used in this study. Colour code: Ni–grey, Fe–pink, S–yellow, N–blue, O–red, C–cyan, H–white.

The structure described above was first optimised using a limited memory algorithm (LBFGS)[34] and then equilibrated for 4 ps while fixing all the C atoms to their initial positions, with the exception of the carbon of CO_2 and of those of the His93 and Lys563 side chains. All molecular dynamics simulations were performed in the NVT ensemble with a Nosé-Hoover thermostat[35] set at 300 K. A time step of 0.5 fs was used to integrate the equations of motion. The constraints on the C atoms were kept during the simulations. To avoid fictitious rotations of the His93 ring that would be precluded in a full protein model, we fixed the two N and H atoms of the imidazole ring that are furthest to CO_2, which maintained the correct alignment between the ring and the CO_2 plane. It is known that the correlation effects in transition metals represent a challenge for DFT[36]. Adopting a Hubbard approach[37] as done for other Fe–S clusters[38,39], with an effective parameter equal to 2 eV, resulted into a C-cluster geometry that better matched X-ray diffraction data[11].

We adopted metadynamics to sample the free energy landscapes[40,41]. Provided that the collective variables (CVs) are carefully chosen, metadynamics allows to escape a free energy minimum and therefore to estimate the activation free energy of the process[42,43]. With the exception of the run in section 3.1, which was stopped when the CV did not sample around either minimum any more, all the metadynamics simulations were stopped when the system overcame the free energy barrier of interest. Gaussians were deposited every 30 steps. The optimal width of the Gaussians was chosen to match the typical variation of the CVs. Additional metadynamics details can be found in the Supplementary Information.

3 Results and discussion

3.1 Binding of CO_2 to the C-cluster

Figure 2 shows the last snapshot of the 4ps equilibration. During the trajectory, the CO_2 molecule remains bent at an average bond angle of 118° that is typi-

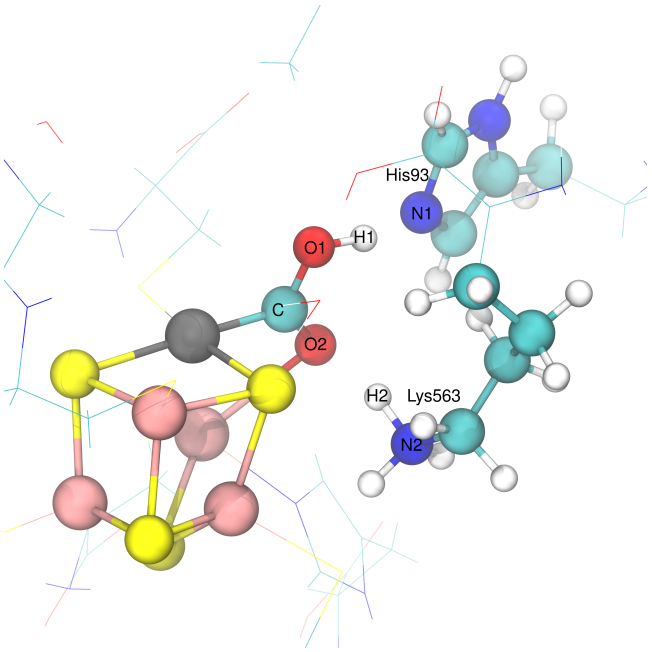

Figure 2: Structures of the C-cluster and the surrounding protein after equilibration. The C-cluster, the COOH ligand, and the side chains of His93 and Lys563 are shown in the ball-and-stick representation. Colour code: Ni–grey, Fe–pink, S–yellow, N–blue, O–red, C–cyan, H–white.

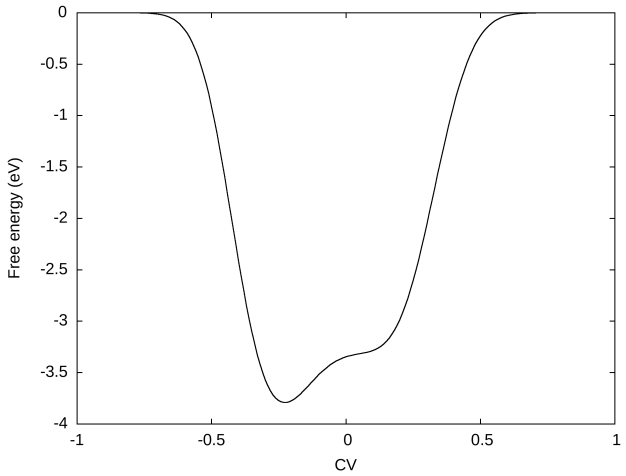

Figure 3: Free energy profile as a function of the CV defined as the difference between n(N1–H1) and n(O2–H2) (atom labels correspond to those of Figure 2). The minimum at around –0.25 corresponds to the structure in Figure 2.

cal of Ni–COOH complexes[44]. In addition, the hydrogen bond interactions with His93 (between H1 and N1) and Lys563 (between H2 and O2) are preserved[12,45]. We observe that a proton transfer from His93 to CO_2 has occurred during the equilibration, with the formation of a COOH ligand that X-ray diffraction cannot detect. Histidine has a pKa of about 6, but it is difficult to estimate the exact pKa of His93, as the variability of pKa increases with histidine burial within the protein[46]. Because of its acid-base properties, Drennan *et al.* have suggested that histidine can be the species donating a proton to the Ni-bound carboxylate[7]. However, while Breglia *et al.* have recently reported the spontaneous H^+ transfer from His93 to the OH^- ligand in the unbound form of the C-cluster[47], a COOH ligand has not been previously found by computational studies. We conclude that DFT optimisations, including the one that we carried out before equilibration, cannot capture the H^+ transfer to CO_2, which highlights the importance of temperature effects in the present study.

We ran 4 ps of metadynamics to establish the stability of the structure in Figure 2 with respect to the pre-equilibrated configuration. The coordination number of N1 with respect to H1, n(N1–H1), can be defined as

$$n(\text{N1–H1}) = \frac{1-(r/r_0)^6}{1-(r/r_0)^{12}}, \quad (1)$$

where r is the distance between the atoms and r_0 the average value of 1.02 Å. A similar definition applies to n(O2–H2). The free energy profile as a function of the CV defined as the difference between n(N1–H1) and n(O2–H2) is plotted in Figure 3. It confirms that the configuration where a CO_2 ligand interacts with a charged His93 is not the most stable at room temperature, while a COOH ligand is formed instead. This finding will have implications for the reaction mechanism catalysed by the C-cluster.

3.2 Exploring the free energy landscapes

It is generally assumed that the conversion of CO_2 starts with the protonation of O2 by the neighbouring His93, which triggers the subsequent breaking of the C–O2 bond (see Figure 2 for atom labels)[11,25]. The COOH ligand, however, makes the O2 protonation unlikely. In search of relevant intermediates, we spanned the reaction coordinate of the C–O2 distance (CV1) by metadynamics. Interestingly, we noted that as the C–O2 bond is weakened by the biased potential, Lys563 transfers its H2 ion to O2. We note that the acidic role of Lys563 in the protonation of O2 has been suggested by recent DFT investigations[26,48]. This event is followed by the internal transfer of the H1 ion to O2, mediated by N1 of His93, with the subsequent formation of water.

These findings prompted us to explore the free energy surface with the addition of a second CV, namely the distance between O2 and H1 (CV2). After 2 ps of metadynamics, both the H^+ transfers described above consistently occur, with the second being facilitated by the breaking of the Fe–O2 bond. The formed water molecule diffuses along CV1, as indicated by the free energy surface in the upper panel of Figure 4. The step has an activation free energy of 0.8 eV.

At the end of the metadynamics run, the system was equilibrated for 2 ps.

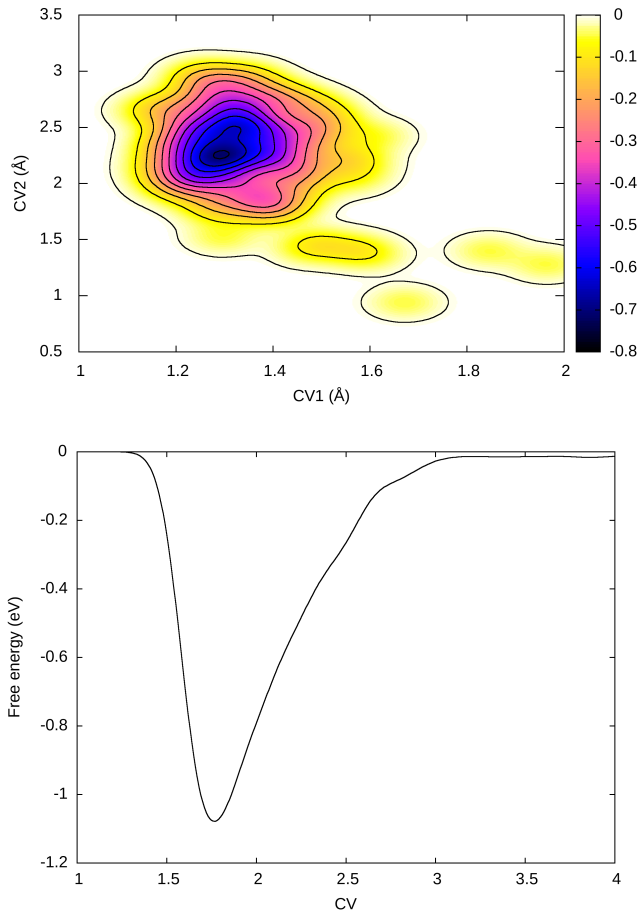

Figure 4: Upper panel: Free energy surface as a function of the C–O2 and O2–H1 distances, CV1 and CV2, respectively (see Figure 2). Lower panel: Free energy surface as a function of the Ni–C distance, CV (see upper panel of Figure 5).

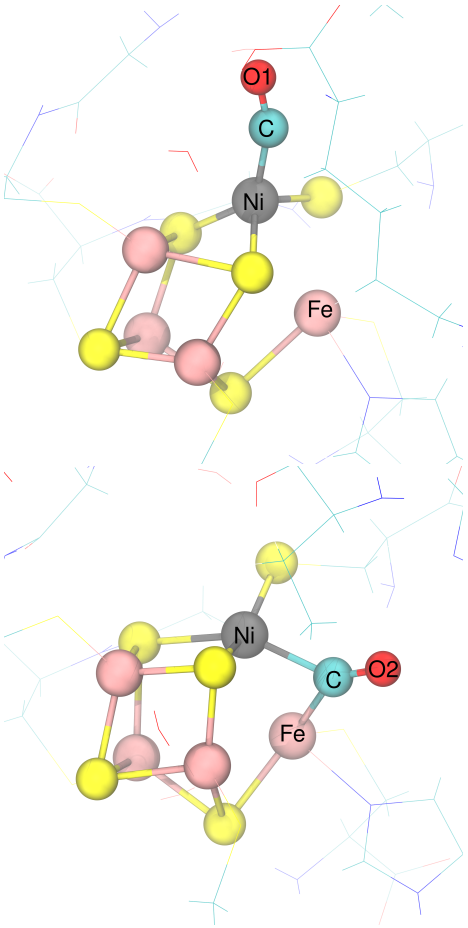

Figure 5: Intermediate structures of the C-cluster with the CO molecule bound in monodentate (upper panel) and bridging (lower panel) configurations that result from the two mechanisms explored. Colour code: Ni–grey, Fe–pink, S–yellow, N–blue, O–red, C–cyan, H–white.

The upper panel of Figure 5 shows a representative snapshot of the equilibration trajectory. The CO carbon binds in a monodentate fashion the Ni atom. The resulting tetrahedral configuration has been reported for the C-cluster with CO[9] or *n*-butyl isocyanate[49] bound.

We used the structure in the upper panel of Figure 5 as the initial geometry of a 5 ps metadynamics run aimed at calculating the binding free energy of CO, using the Ni–C distance as CV. The free energy along the CV is plotted in the lower panel of Figure 4, from which we estimate that the binding free energy is around 1.1 eV.

Figure 2 points towards a mechanism where a water molecule is released first, which leaves the C-cluster with a bound CO, as reported for the reduction of CO_2 by synthetic Fe_4S_4 clusters[50]. Thus, we have considered an alternative mechanism where Lys563 transfers its proton to the O1 atom of the COOH ligand to eliminate a water molecule. We have chosen as CV1 the distance between O1 and H2, and as CV2 the distance between C and O1. To confine the sampling to the region of most interest and avoid fluctuations of the Lys563 side chain that would be precluded in the full protein, we have inserted a Gaussian wall, with height of 1 eV and width of 0.05 Å, at 4.5 Å along CV1.

The upper panel of Figure 6 shows the free energy surface as a function of the two CVs. An energetic cost of 0.6 eV, which is lower by 0.2 eV than that of the previous mechanism, is required for the system to escape the minimum of Figure 3. When this happens, the formed water molecule diffuses, as shown by the free energy profile along CV2. Thus, after 4ps and with the resulting CO molecule bound to the C-cluster, the metadynamics was stopped and the system equilibrated for 3 ps.

A representative snapshot of the equilibrated system is presented in the lower panel of Figure 5. In contrast to the previous mechanism, we do not observe a tetrahedral coordination, but a distorted square planar geometry of Ni. In addition to the Ni–C, a Fe–C bond stabilises the binding of CO, now in a bridging configuration, to the C-cluster. CO is isoelectronic to CN^-, which

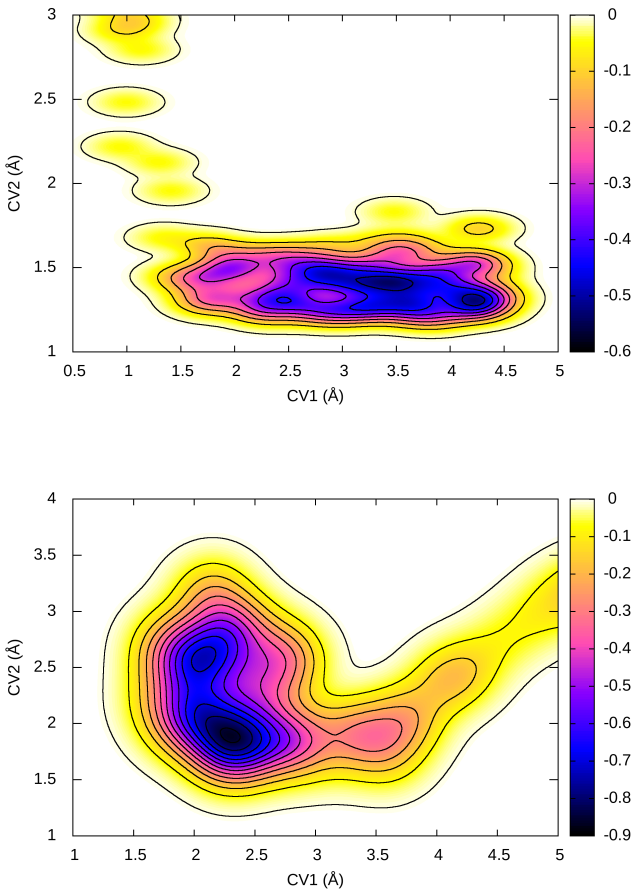

Figure 6: Upper panel: Free energy surface as a function of the O1–H2 and C–O1 distances, CV1 and CV2, respectively (see Figure 2). Lower panel: Free energy surface as a function of the Fe–C and Ni–C distances, CV1 and CV2, respectively (see lower panel of Figure 5).

represents an inhibitor of the reverse oxidation reaction catalysed by CODH[51,52]. In the crystal structure reported by Jeoung *et al.*, CN^- binds to an empty site of Ni, thus completing its square planar coordination geometry[12]. The Ni atom of the intermediate in the lower panel of Figure 5 has a similar geometry. Gong *et al.* have suggested that a change from square planar to tetrahedral geometry occurs during the reaction catalysed by the C-cluster[16]. By comparing the two geometries of Ni in Figure 5, we conclude that the key factor that determines them is the reaction pathway. In particular, if O2 is the oxygen atom that is released with H_2O, then the result is a tetrahedral Ni, whereas a distorted square planar geometry is the consequence of O1 elimination.

To calculate the binding free energy of the bridging CO molecule, we ran 2 ps of metadynamics, using the Fe–C and Ni–C distances as CV1 and CV2, respectively. The lower panel of Figure 6 shows the corresponding free energy landscape. The detachment of the CO molecule proceeds via the initial breaking of the Fe–C bond, followed by that of the Ni–C bond, with a dynamics that is entirely consistent with the apical direction of the CO gas tunnel with respect to the Ni square planar coordination[25]. The estimated free energy required for the molecule to start to diffuse is about 0.9 eV, lower by 0.2 eV than that of a monodentate CO binding.

3.3 Catalytic mechanism of CODH

The insights offered by the metadynamics simulations led us to revisit the catalytic mechanism of CODH, whose steps we have now revised in Figure 7. C_{red2} corresponds to the reduced structure observed by X-ray diffraction (intermediate I)[11]. The exchange of H_2O for CO_2 leads to the formation of the most stable COOH ligand that interacts by hydrogen bonds with the surrounding His93 and Lys563 residues (intermediate II). We stress that both His93 and Lys563 are located on top of a possible tunnel connecting the C-cluster to the external solvent that would be an ideal path for the required proton transfers[7]. The charged side chain of Lys563 can also form a hydrogen bond with the OH

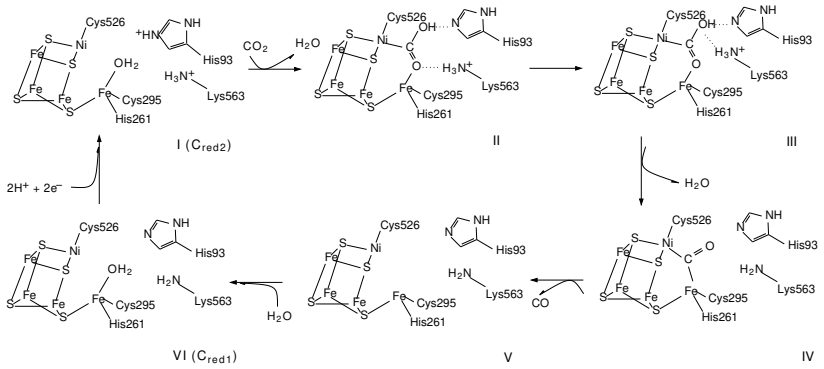

Figure 7: Revised catalytic mechanism of CO_2 reduction at the C-cluster.

group of the ligand (intermediate III), which drives the elimination of H_2O. In the resulting structure, CO binds the C-cluster in a bridging fashion (intermediate IV). The next step is the elimination of CO through the gas tunnel (intermediate V), which is followed by the binding of a water molecule at the Fe site in the C_{red1} state (intermediate VI)[11]. The cycle is completed with the transfer of two protons to His93 and Lys563 and two electrons to the C-cluster, which re-forms C_{red2}. Given that the free energy barrier for the CO_2 binding to the C-cluster is around 0.5 eV[53] and that the formation of H_2O requires 0.6 eV, the elimination of CO is the rate limiting step of the cycle, with a free energy cost of around 0.9 eV. This value, however, is likely to be reduced by the possible involvement of the water molecule that substitutes CO at the external Fe atom. The mechanism in Figure 7 clarifies the crucial roles of His93 and Lys563, in line with the abolished activity of the enzyme when the two residues are changed to alanine[54].

4 Conclusions

We have presented an *ab initio* metadynamics investigation of the mechanism of reduction of CO_2 to CO catalysed by CODH. We found that the ligand that binds the reduced state of the C-cluster is COOH, which has significant implica-

tions for the reaction pathway to CO. In particular, the release of CO, which we predict to be the rate-limiting step of the cycle, can occur only after that of H_2O. We have also shown that the different Ni geometries reported experimentally can be rationalised by considering which oxygen atom of COOH is eliminated with H_2O. Finally, we have provided evidence of the crucial role of His93 and Lys563, which are suggested to be terminal elements of proton shuttles that are involved at different steps of the reaction. By reconciling our results with previous experimental observations, we have proposed a revised catalytic cycle that advances our understanding of this fascinating class of enzymes.

Acknowledgements

Via our membership of the UK's HEC Materials Chemistry Consortium, which is funded by EPSRC (EP/L000202, EP/R029431), this work used the ARCHER UK National Supercomputing Service (http://www.archer.ac.uk). All data supporting this study (the XYZ coordinates of all structures and the metadynamics hills output) is provided as Supplementary Information accompanying this paper.

References

(1) Wang, W.; Wang, S.; Ma, X.; Gong, J. Recent advances in catalytic hydrogenation of carbon dioxide. *Chem. Soc. Rev.* **2011**, *40*, 3703–3727.

(2) Appel, A. M.; Bercaw, J. E.; Bocarsly, A. B.; Dobbek, H.; DuBois, D. L.; Dupuis, M.; Ferry, J. G.; Fujita, E.; Hille, R.; Kenis, P. J., et al. Frontiers, opportunities, and challenges in biochemical and chemical catalysis of CO2 fixation. *Chem. Rev.* **2013**, *113*, 6621–6658.

(3) Zheng, T.; Jiang, K.; Wang, H. Recent advances in electrochemical CO2-to-CO conversion on heterogeneous catalysts. *Adv. Mater.* **2018**, *30*, 1802066.

(4) Can, M.; Armstrong, F. A.; Ragsdale, S. W. Structure, function, and mechanism of the nickel metalloenzymes, CO dehydrogenase, and acetyl-CoA synthase. *Chem. Rev.* **2014**, *114*, 4149–4174.

(5) Shin, W.; Lee, S. H.; Shin, J. W.; Lee, S. P.; Kim, Y. Highly Selective Electrocatalytic Conversion of CO2 to CO at- 0.57 V (NHE) by Carbon Monoxide Dehydrogenase from Moorella t hermoacetica. *J. Am. Chem. Soc.* **2003**, *125*, 14688–14689.

(6) Parkin, A.; Seravalli, J.; Vincent, K. A.; Ragsdale, S. W.; Armstrong, F. A. Rapid and efficient electrocatalytic CO2/CO interconversions by Carboxydothermus hydrogenoformans CO dehydrogenase I on an electrode. *J. Am. Chem. Soc.* **2007**, *129*, 10328–10329.

(7) Drennan, C. L.; Heo, J.; Sintchak, M. D.; Schreiter, E.; Ludden, P. W. Life on carbon monoxide: X-ray structure of Rhodospirillum rubrum Ni-Fe-S carbon monoxide dehydrogenase. *Proc. Natl. Acad. Sci. U. S. A.* **2001**, *98*, 11973–11978.

(8) Dobbek, H.; Svetlitchnyi, V.; Gremer, L.; Huber, R.; Meyer, O. Crystal structure of a carbon monoxide dehydrogenase reveals a [Ni-4Fe-5S] cluster. *Science* **2001**, *293*, 1281–1285.

(9) Darnault, C.; Volbeda, A.; Kim, E. J.; Legrand, P.; Vernède, X.; Lindahl, P. A.; Fontecilla-Camps, J. C. Ni-Zn-[Fe 4-S 4] and Ni-Ni-[Fe 4-S 4] clusters in closed and open α subunits of acetyl-CoA synthase/carbon monoxide dehydrogenase. *Nat. Struct. Mol. Biol.* **2003**, *10*, 271–279.

(10) Dobbek, H.; Svetlitchnyi, V.; Liss, J.; Meyer, O. Carbon Monoxide Induced Decomposition of the Active Site [Ni- 4Fe- 5S] Cluster of CO Dehydrogenase. *J. Am. Chem. Soc.* **2004**, *126*, 5382–5387.

(11) Jeoung, J.-H.; Dobbek, H. Carbon dioxide activation at the Ni, Fe-cluster of anaerobic carbon monoxide dehydrogenase. *Science* **2007**, *318*, 1461–1464.

(12) Jeoung, J.-H.; Dobbek, H. Structural basis of cyanide inhibition of Ni, Fe-containing carbon monoxide dehydrogenase. *J. Am. Chem. Soc.* **2009**, *131*, 9922–9923.

(13) Conover, R. C.; Park, J. B.; Adams, M. W.; Johnson, M. K. Formation and properties of an iron-nickel sulfide (NiFe3S4) cluster in Pyrococcus furiosus ferredoxin. *J. Am. Chem. Soc.* **1990**, *112*, 4562–4564.

(14) Lindahl, P. A. The Ni-containing carbon monoxide dehydrogenase family: light at the end of the tunnel? *Biochemistry* **2002**, *41*, 2097–2105.

(15) Rebelein, J. G.; Stiebritz, M. T.; Lee, C. C.; Hu, Y. Activation and reduction of carbon dioxide by nitrogenase iron proteins. *Nat. Chem. Biol.* **2017**, *13*, 147–149.

(16) Gong, W.; Hao, B.; Wei, Z.; Ferguson, D. J.; Tallant, T.; Krzycki, J. A.; Chan, M. K. Structure of the $\alpha 2\varepsilon 2$ Ni-dependent CO dehydrogenase component of the Methanosarcina barkeri acetyl-CoA decarbonylase/synthase complex. *Proc. Natl. Acad. Sci. U. S. A.* **2008**, *105*, 9558–9563.

(17) Woolerton, T. W.; Sheard, S.; Reisner, E.; Pierce, E.; Ragsdale, S. W.; Armstrong, F. A. Efficient and clean photoreduction of CO2 to CO by enzyme-modified TiO2 nanoparticles using visible light. *J. Am. Chem. Soc.* **2010**, *132*, 2132–2133.

(18) Woolerton, T. W.; Sheard, S.; Pierce, E.; Ragsdale, S. W.; Armstrong, F. A. CO2 photoreduction at enzyme-modified metal oxide nanoparticles. *Energy Environ. Sci.* **2011**, *4*, 2393–2399.

(19) Zhang, L.; Can, M.; Ragsdale, S. W.; Armstrong, F. A. Fast and selective photoreduction of CO2 to CO catalyzed by a complex of carbon monoxide dehydrogenase, TiO2, and Ag nanoclusters. *ACS catalysis* **2018**, *8*, 2789–2795.

(20) Majumdar, A. Bioinorganic modeling chemistry of carbon monoxide dehydrogenases: description of model complexes, current status and possible future scopes. *Dalton Trans.* **2014**, *43*, 12135–12145.

(21) Le, J. M.; Bren, K. L. Engineered Enzymes and Bioinspired Catalysts for Energy Conversion. *ACS Energy Lett.* **2019**, *4*, 2168–2180.

(22) Volbeda, A.; Fontecilla-Camps, J. C. Structural bases for the catalytic mechanism of Ni-containing carbon monoxide dehydrogenases. *Dalton Trans.* **2005**, 3443–3450.

(23) Jeon, W. B.; Singer, S. W.; Ludden, P. W.; Rubio, L. M. New insights into the mechanism of nickel insertion into carbon monoxide dehydrogenase: analysis of Rhodospirillum rubrum carbon monoxide dehydrogenase variants with substituted ligands to the [Fe 3 S 4] portion of the active-site C-cluster. *JBIC, J. Biol. Inorg. Chem.* **2005**, *10*, 903–912.

(24) Seravalli, J.; Ragsdale, S. W. 13C NMR characterization of an exchange reaction between CO and CO2 catalyzed by carbon monoxide dehydrogenase. *Biochemistry* **2008**, *47*, 6770–6781.

(25) Amara, P.; Mouesca, J.-M.; Volbeda, A.; Fontecilla-Camps, J. C. Carbon Monoxide Dehydrogenase Reaction Mechanism: A Likely Case of Abnormal CO2 Insertion to a Ni-H Bond. *Inorg. Chem.* **2011**, *50*, 1868–1878.

(26) Liao, R.-Z.; Siegbahn, P. E. Energetics for the mechanism of nickel-containing carbon monoxide dehydrogenase. *Inorg. Chem.* **2019**, *58*, 7931–7938.

(27) Humphrey, W.; Dalke, A.; Schulten, K. VMD: Visual molecular dynamics. *J. Mol. Graph.* **1996**, *14*, 33–38.

(28) Kühne, T. D.; Iannuzzi, M.; Del Ben, M.; Rybkin, V. V.; Seewald, P.; Stein, F.; Laino, T.; Khaliullin, R. Z.; Schütt, O.; Schiffmann, F., et al. CP2K: An electronic structure and molecular dynamics software package-Quickstep: Efficient and accurate electronic structure calculations. *J. Chem. Phys.* **2020**, *152*, 194103.

(29) Perdew, J. P.; Burke, K.; Ernzerhof, M. Generalized gradient approximation made simple. *Phys. Rev. Lett.* **1996**, *77*, 3865.

(30) VandeVondele, J.; Hutter, J. Gaussian basis sets for accurate calculations on molecular systems in gas and condensed phases. *J. Chem. Phys.* **2007**, *127*.

(31) Goedecker, S.; Teter, M.; Hutter, J. Separable dual-space Gaussian pseudopotentials. *Phys. Rev. B* **1996**, *54*, 1703.

(32) Noodleman, L. Valence bond description of antiferromagnetic coupling in transition metal dimers. *J. Chem. Phys.* **1981**, *74*, 5737–5743.

(33) Spangler, N. J.; Meyers, M. R.; Gierke, K. L.; Kerby, R. L.; Roberts, G. P.; Ludden, P. W. Substitution of valine for histidine 265 in carbon monoxide dehydrogenase from Rhodospirillum rubrum affects activity and spectroscopic states. *J. Biol. Chem.* **1998**, *273*, 4059–4064.

(34) Byrd, R. H.; Lu, P.; Nocedal, J.; Zhu, C. A limited memory algorithm for bound constrained optimization. *SIAM J. Sci. Comput.* **1995**, *16*, 1190–1208.

(35) Nosé, S. A unified formulation of the constant temperature molecular dynamics methods. *J. Chem. Phys.* **1984**, *81*, 511.

(36) Himmetoglu, B.; Floris, A.; Gironcoli, S.; Cococcioni, M. Hubbard-corrected DFT energy functionals: The LDA+U description of correlated systems. *Int. J. Quantum Chem.* **2014**, *114*, 14–49.

(37) Dudarev, S.; Botton, G.; Savrasov, S.; Humphreys, C.; Sutton, A. Electron-energy-loss spectra and the structural stability of nickel oxide: An LSDA+U study. *Phys. Rev. B* **1998**, *57*, 1505–1509.

(38) Nair, N. N.; Ribas-Arino, J.; Staemmler, V.; Marx, D. Magnetostructural Dynamics from Hubbard-U Corrected Spin-Projection:[2Fe- 2S] Complex in Ferredoxin. *J. Chem. Theory Comput.* **2010**, *6*, 569–575.

(39) Terranova, U.; de Leeuw, N. H. Aqueous Fe2S2 cluster: structure, magnetic coupling, and hydration behaviour from Hubbard U density functional theory. *Phys. Chem. Chem. Phys.* **2014**, *16*, 13426–13433.

(40) Laio, A.; Parrinello, M. Escaping free-energy minima. *Proc. Natl. Acad. Sci. U. S. A.* **2002**, *99*, 12562–12566.

(41) Laio, A.; Rodriguez-Fortea, A.; Gervasio, F. L.; Ceccarelli, M.; Parrinello, M. Assessing the Accuracy of Metadynamics. *J. Phys. Chem. B* **2005**, *109*, PMID: 16851755, 6714–6721.

(42) Laio, A.; Gervasio, F. L. Metadynamics: a method to simulate rare events and reconstruct the free energy in biophysics, chemistry and material science. *Rep. Progr. Phys.* **2008**, *71*, 126601.

(43) Farkas, B.; Terranova, U.; De Leeuw, N. H. Binding modes of carboxylic acids on cobalt nanoparticles. *Phys. Chem. Chem. Phys.* **2020**, *22*, 985–996.

(44) Yoo, C.; Kim, J.; Lee, Y. Synthesis and Reactivity of Nickel (II) Hydroxycarbonyl Species, NiCOOH-κ C. *Organometallics* **2013**, *32*, 7195–7203.

(45) Fesseler, J.; Jeoung, J.-H.; Dobbek, H. How the [NiFe4S4] cluster of CO dehydrogenase activates CO2 and NCO-. *Angew. Chem. Int. Ed.* **2015**, *54*, 8560–8564.

(46) Edgcomb, S. P.; Murphy, K. P. Variability in the pKa of histidine side-chains correlates with burial within proteins. *Proteins: Struct., Funct., Genet.* **2002**, *49*, 1–6.

(47) Breglia, R.; Arrigoni, F.; Sensi, M.; Greco, C.; Fantucci, P.; De Gioia, L.; Bruschi, M. First-Principles Calculations on Ni,Fe-Containing Carbon Monoxide Dehydrogenases Reveal Key Stereoelectronic Features for Binding and Release of CO2 to/from the C-Cluster. *Inorg. Chem.* **2021**, *60*, 387–402.

(48) Siegbahn, P. E. A quantum chemical approach for the mechanisms of redox-active metalloenzymes. *RSC Adv.* **2021**, *11*, 3495–3508.

(49) Jeoung, J.-H.; Dobbek, H. n-Butyl isocyanide oxidation at the [NiFe 4 S 4 OH x] cluster of CO dehydrogenase. *JBIC, J. Biol. Inorg. Chem.* **2012**, *17*, 167–173.

(50) Stiebritz, M. T.; Hiller, C. J.; Sickerman, N. S.; Lee, C. C.; Tanifuji, K.; Ohki, Y.; Hu, Y. Ambient conversion of CO 2 to hydrocarbons by biogenic and synthetic [Fe 4 S 4] clusters. *Nat. Catal.* **2018**, *1*, 444–451.

(51) Ciaccafava, A.; Tombolelli, D.; Domnik, L.; Fesseler, J.; Jeoung, J.-H.; Dobbek, H.; Mroginski, M. A.; Zebger, I.; Hildebrandt, P. When the inhibitor tells more than the substrate: the cyanide-bound state of a carbon monoxide dehydrogenase. *Chem. Sci.* **2016**, *7*, 3162–3171.

(52) Ciaccafava, A.; Tombolelli, D.; Domnik, L.; Jeoung, J.-H.; Dobbek, H.; Mroginski, M.-A.; Zebger, I.; Hildebrandt, P. Carbon monoxide dehydrogenase reduces cyanate to cyanide. *Angew. Chem., Int. Ed.* **2017**, *56*, 7398–7401.

(53) Wang, P.-h.; Bruschi, M.; De Gioia, L.; Blumberger, J. Uncovering a dynamically formed substrate access tunnel in carbon monoxide dehydrogenase/acetyl-CoA synthase. *J. Am. Chem. Soc.* **2013**, *135*, 9493–9502.

(54) Kim, E. J.; Feng, J.; Bramlett, M. R.; Lindahl, P. A. Evidence for a proton transfer network and a required persulfide-bond-forming cysteine residue in Ni-containing carbon monoxide dehydrogenases. *Biochemistry* **2004**, *43*, 5728–5734.